

# Improved EEG Source Localization with Bayesian Uncertainty Modelling of Unknown Skull Conductivity

Ville Rimpiläinen<sup>a,h,\*</sup>, Alexandra Koulouri<sup>b,c</sup>, Felix Lucka<sup>d,e</sup>, Jari P. Kaipio<sup>f,g</sup>,  
Carsten H. Wolters<sup>h</sup>

<sup>a</sup>*Department of Physics, University of Bath, Claverton Down, Bath BA2 7AY, The United Kingdom*

<sup>b</sup>*Laboratory of Mathematics, Tampere University of Technology, P. O. Box 692, 33101 Tampere, Finland*

<sup>c</sup>*Department of Physics, Aristotle University of Thessaloniki, Thessaloniki 541 24, Greece*

<sup>d</sup>*Computational Imaging, Centrum Wiskunde & Informatica, Science Park 123, 1098 XG Amsterdam, The Netherlands*

<sup>e</sup>*Centre for Medical Image Computing, University College London, Gower Street, London WC1E 6BT, The United Kingdom*

<sup>f</sup>*Department of Mathematics, University of Auckland, Private bag 92019, Auckland 1142, New Zealand*

<sup>g</sup>*Department of Applied Physics, University of Eastern Finland, FI-90211 Kuopio, Finland*

<sup>h</sup>*Institute for Biomagnetism and Biosignalanalysis, University of Münster, Malmedyweg 15, D-48149 Münster, Germany*

---

## Abstract

Electroencephalography (EEG) source imaging is an ill-posed inverse problem that requires accurate conductivity modelling of the head tissues, especially the skull. Unfortunately, the conductivity values are difficult to determine *in vivo*. In this paper, we show that the exact knowledge of the skull conductivity is not always necessary when the Bayesian approximation error (BAE) approach is exploited. In BAE, we first postulate a probability distribution for the skull conductivity that describes our (lack of) knowledge on its value, and model the effects of this uncertainty on EEG recordings with the help of an additive error term in the observation model. Before the Bayesian inference, the likelihood is marginalized over this error term. Thus, in the inversion we estimate only our primary unknown, the source distribution. We quantified the improvements in the source localization when the proposed Bayesian modelling was used in the presence of different skull conductivity errors and levels of measurement noise. Based on the results, BAE was able to improve the source localization accuracy, particularly when the unknown (true) skull conductivity was much lower than

---

\*Corresponding author  
Preprint submitted to *NeuroImage*  
Email address: [vrimpila@gmail.com](mailto:vrimpila@gmail.com) (Ville Rimpiläinen)

the expected standard conductivity value. The source locations that gained the highest improvements were shallow and originally exhibited the largest localization errors. In our case study, the benefits of BAE became negligible when the signal-to-noise ratio dropped to 20 dB.

*Keywords:* Electroencephalography, uncertainty modelling, Bayesian inverse problem, skull conductivity, source localization

---

## 20 1. Introduction

Electroencephalography (EEG) is a routinely used brain imaging modality to study cognitive states of the brain and to diagnose, for example, epilepsy and brain dysfunction. The EEG data is recorded by measuring electric potentials on the scalp that are induced by electric current sources in the brain [1]. EEG  
25 is relatively easy to use, low-cost, it has high temporal resolution, and the apparatus is small compared to magnetoencephalography (MEG) or magnetic resonance imaging (MRI) equipment.

The mapping that translates the neuronal current sources into EEG measurements is called the forward model. The inversion of this mapping, i.e., source  
30 reconstruction from EEG data, is an ill-posed inverse problem, and stable estimates cannot be computed from noisy measurements without either regularization or by employing prior models. Additionally, the solution depends strongly on such forward model parameters as the geometry of the head [2, 3, 4, 5, 6, 7, 8] and the electric conductivities of the head tissues [9, 10, 11, 12, 13, 14]. Especially  
35 the accurate conductivity modelling of the skull has been shown to be essential for accurate source reconstructions [9, 12, 5, 13, 15, 16].

Usually, the geometry can be extracted sufficiently by using such auxiliary imaging tools as MRI and in some clinical cases computed tomography (CT) [17]. However, there are only few techniques to determine or calibrate tissue  
40 conductivities *in vivo*. These techniques usually utilize either well defined somatosensory evoked potentials / fields (SEP/SEF) in combination with EEG [18, 19], EEG/MEG [20, 21, 22, 23, 24] or electrical impedance tomography

(EIT) [25, 26, 27]. Unfortunately, these measurements may not always be available or cannot be conducted. Moreover, even if SEP/SEF data were available  
45 for the calibration, the resulting skull conductivity value might not be optimal for sources in another brain region [19].

In this paper, we propose to use a Bayesian approximation error (BAE) approach [28, 29] to consider the unknown skull conductivity. In BAE, the observation model is formulated using a standard forward model accompanied  
50 with an additive approximation error term that encompasses the effects of the skull conductivity uncertainty. Before the Bayesian inference, this approximation error term is marginalized from the likelihood using a Gaussian approximation. Thus, the marginalized likelihood includes statistical knowledge of both the approximation error and measurement noise, and in the inversion only the  
55 unknown source configuration is solved.

The approximation error statistics are pre-computed from Monte Carlo simulations. In practice, we postulate a probability distribution for the skull conductivity and generate a set of lead field models based on this distribution. By using these *sample* models, we estimate the statistics of the approximation error  
60 term, i.e., the statistics of the discrepancies in the EEG recordings with respect to a *standard* model with a fixed skull conductivity. The posterior results from the marginalized likelihood and prior distribution of choice. The maximum-a-posteriori (MAP) estimate can be used for source visualization. Previously, the BAE approach has been successfully used, for example, in EIT [30, 31, 32] and  
65 optical tomography [33, 34, 35]. In EEG source imaging, the BAE approach has been shown to alleviate localization errors arising from the unknown head geometry by using simulated 2-dimensional finite element (FE) models [36].

In the current study, we present a comprehensive analysis of the performance of the BAE approach in improving the source localization when the skull conductivity is unknown. We quantify the effects of the unknown skull conductivity by  
70 evaluating the corresponding approximation errors in the EEG recordings and the source localization errors in the reconstructions. Subsequently, we quantify the improvements in the source localization when the proposed Bayesian mod-

elling is used in the presence of different skull conductivity errors and levels of  
75 measurement noise. This work is a simulation study that is carried out by using  
3-dimensional FE-based head models.

## 2. Theory

### 2.1. Bayesian framework with linear forward model

The computational domain is denoted with  $\Omega$  and its electric conductivity  
80 with  $\sigma(x)$  where  $x \in \Omega$ . For numerical implementations, the domain is dis-  
cretized and the observation model is written as

$$v = A(\sigma)d + e, \quad (1)$$

where  $v \in \mathbb{R}^m$  are the measurements,  $m$  is the number of measurements,  $A(\sigma) \in$   
 $\mathbb{R}^{m \times 3n}$  is the lead field matrix that depends on electric conductivity  $\sigma$ ,  $d \in$   
 $\mathbb{R}^{3n}$  is the distributed dipole source configuration and  $e \sim \mathcal{N}(e_*, \Gamma_e)$  is the  
85 measurement noise. The noise covariance matrix is modelled as  $\Gamma_e = \tilde{\Gamma}_e +$   
 $\gamma I$  where the small diagonal matrix  $\gamma I$  ensures that the level of noise is not  
underestimated.

In the Bayesian framework, the inverse solution is formally the posterior  
density of the Bayes formula [28, 37, 38]. Here, we consider the posterior that  
90 is the probability density of different source configurations given that the EEG  
measurements are known

$$\pi(d|v) \propto \pi(v|d)\pi(d), \quad (2)$$

where  $\pi(v|d)$  is the likelihood and  $\pi(d)$  the prior.

For the observation model, Equation (1), the likelihood model can be written  
as

$$\pi(v|d) \propto \exp\left(-\frac{1}{2}(v - Ad - e_*)^T \Gamma_e^{-1} (v - Ad - e_*)\right). \quad (3)$$

95 Note that the model  $A(\sigma) = A$  assumes that the accurate values of electric  
conductivities of the patient are known which in practice, without additional  
effort, is almost never the case.

## 2.2. Bayesian uncertainty modelling

In BAE, we re-write the observation model with the help of an approximate  
 100 lead field,  $A(\sigma_0) = A_0$ , in which we employ standard fixed values for the electric  
 conductivity,  $\sigma_0$ . We can re-write

$$v = A_0 d + \varepsilon + e, \quad (4)$$

where  $\varepsilon = Ad - A_0 d$  is the *approximation error*,  $\varepsilon \in \mathbb{R}^m$ , induced by the use of  
 the approximate model. The approximation error is a random variable (vector)  
 whose distribution is determined by the joint (prior) distribution  $\pi(\sigma, d)$ .

105 We further approximate that  $\varepsilon \sim \mathcal{N}(\varepsilon_*, \Gamma_\varepsilon)$ ,  $e$  and  $d$  are uncorrelated, i.e.,  $\varepsilon$   
 is considered as another random additive error term. This specific BAE model  
 is sometimes referred to as enhanced error model [28, 39, 29]. Even though, in  
 practice,  $\varepsilon$  and  $d$  are usually correlated, this approximation often leads to very  
 similar inverse solutions [28, 39, 29]. In our case, since we assume that the true  
 110 source activity  $d$  is focal (sparse), the cross-covariances with  $\varepsilon$  will be negligible.

Based on these approximations, we formulate the probability distribution of  
 the likelihood as

$$\pi(v|d) \propto \exp\left(-\frac{1}{2}(v - A_0 d - \varepsilon_* - e_*)^\top (\Gamma_\varepsilon + \Gamma_e)^{-1} (v - A_0 d - \varepsilon_* - e_*)\right). \quad (5)$$

In the case of Gaussian additive measurement errors,  $e \sim \mathcal{N}(e_*, \Gamma_e)$ , we can  
 quantitatively define the case when the approximation errors dominate mea-  
 115 surement errors as

$$\|e_*\|^2 + \text{tr } \Gamma_e < \|\varepsilon_*\|^2 + \text{tr } \Gamma_\varepsilon \quad (6)$$

and

$$e_{*,k}^2 + \text{var}(e_k) < \varepsilon_{*,k}^2 + \text{var}(\varepsilon_k), \quad (7)$$

where  $\text{tr}(\cdot)$  is the trace of a matrix and  $k = 1, \dots, m$  [29]. When these conditions  
 hold, BAE can be expected to improve the reconstruction results. We shall  
 discuss this further in Section 5.3.

120 *2.3. Maximum a posteriori estimates*

In this paper, we compute maximum a posteriori (MAP) estimates of the posterior

$$\hat{d} = \arg \max_d \pi(d|v) = \arg \max_d \{\pi(v|d)\pi(d)\}. \quad (8)$$

For comparison, we compute three different MAP estimates using three different likelihood models. We refer to these likelihood models as *accurate*, *standard* and *BAE model*, and we describe them in the following. 125

In the *accurate* likelihood model, we assume that the electrical conductivities are accurately known. Since we study here only single dipole source cases, we can write the MAP estimate based on the accurate likelihood model (3) as follows

$$\begin{aligned} \hat{d}_{\text{ACC}} &= \min_d \{\|L_e(v - Ad - e_*)\|_2^2\} \\ \text{s.t.} \quad &\|d_i\| \cdot \|d_j\| = 0 \quad \forall i \neq j, \end{aligned} \quad (9)$$

130 where  $L_e$  is a matrix square root (e.g. Cholesly factor) of  $\Gamma_e^{-1} = L_e^T L_e$ , and  $\|d_i\| = \sqrt{(d_{ix}^2 + d_{iy}^2 + d_{iz}^2)}$  is the strength of the dipole source at node  $i$ . In practice, we minimize the functional for each source space node (considering that in every other node the dipoles are zero) and choose the dipole that achieves the smallest residual as the solution (a.k.a. single dipole scan algorithm) [40, 41].

135 If we, however, compute the solution using the fixed *standard* electrical conductivity values ( $\sigma_0$ ) in the model we get

$$\begin{aligned} \hat{d}_{\text{STAN}} &= \min_d \{\|L_e(v - A_0d - e_*)\|_2^2\} \\ \text{s.t.} \quad &\|d_i\| \cdot \|d_j\| = 0 \quad \forall i \neq j. \end{aligned} \quad (10)$$

From the likelihood of the BAE (5), the source configuration can be estimated as

$$\begin{aligned} \hat{d}_{\text{BAE}} &= \min_d \{\|L_{\varepsilon+e}(v - A_0d - \varepsilon_* - e_*)\|_2^2\} \\ \text{s.t.} \quad &\|d_i\| \cdot \|d_j\| = 0 \quad \forall i \neq j, \end{aligned} \quad (11)$$

where  $(\Gamma_\varepsilon + \Gamma_e)^{-1} = L_{\varepsilon+e}^T L_{\varepsilon+e}$ . Note that the BAE result is computed using the 140 same lead field matrix as in the standard model, Equation (10). Moreover, it is

worth noting that the only differences between (11) and (10) are the subtraction with  $\varepsilon_*$  and that  $L_e$  is replaced with  $L_{\varepsilon+e}$ . This means that the computational complexity is essentially the same when solving (11) and (10).

### 3. Materials and methods

#### 145 3.1. Head models

The geometry of the head was constructed based on T1- and T2-weighted magnetic resonance images of a healthy subject measured with a 3 T MR-scanner. The scalp, eyes, skull compacta, skull spongiosa, cerebrospinal fluid (CSF), gray matter (GM) and white matter (WM) were segmented, for more  
150 details see [42, 14]. In the simulation set-up, 74 measurement electrodes were attached to the scalp, and the one closest to the right-hand-side ear was used as a reference.

The electric conductivities (in S/m) of the different tissues were 0.43 for the scalp [43, 9], 0.505 for the eyes [44], 1.79 for the CSF [45], 0.14 for the WM [44]  
155 and 0.33 for the GM [44]. The skull conductivities of the different head models were the following:

First, we created 200 head models with skull conductivity drawn from a Gaussian distribution with mean  $\sigma_0 = 0.01855$  S/m and standard deviation  $\delta_{\sigma_0} = 0.007225$  S/m. This distribution was set in such a way that the two  
160 standard deviation lower ( $\sigma_0 - 2\delta_{\sigma_0}$ ) and upper ( $\sigma_0 + 2\delta_{\sigma_0}$ ) values were 0.0041 [46, 23, 20, 47] and 0.033 [48], respectively. We refer to these head models as *sample* head models.

Because the skull conductivity variations were assumed to be symmetrically around the mean value  $\sigma_0 = 0.01855$  S/m, we chose to use  $\sigma_0$  in the *standard*  
165 head model and BAE. The skull spongiosa conductivities in all models were selected based on the spongiosa:compacta conductivity ratio 3.6:1 [49, 23].

The head geometry was discretized using a conforming tetrahedral FEM approach. For the forward simulations, the source space that covered the GM was constructed with 30,105 nodes on a regular grid with grid size 2 mm. For the

170 inverse computations, a source space that covered the GM consisted of 10,782  
 source locations on a regular grid with grid size 3 mm. The forward source space  
 was chosen in such a way that it did not contain the same coordinate points as  
 the inverse source space. The lead field matrices used in the simulations were  
 computed using standard piecewise linear FE basis functions with the Saint  
 175 Venant source modelling approach [47, 50].

### 3.2. Computation of the approximation error statistics

The approximation error statistics were created by first choosing randomly  
 one of the sample head models, evaluating the model with randomly chosen  
 source configuration, and finally calculating the approximation error by evalu-  
 180 ating the standard model with the same source configuration,

$$\varepsilon^{(j)} = A(\sigma^{(j)})d^{(j)} - A_0d^{(j)}, \quad (12)$$

where  $A(\sigma^{(j)})$  is one of the sample models,  $d^{(j)}$  random source configuration  
 and  $A_0$  is the standard model.

The procedure was repeated  $J = 200,000$  times, and these simulated error  
 samples were used to calculate the sample mean,  $\varepsilon_*$ , and the sample covariance,  
 185  $\Gamma_\varepsilon$ , of the approximation error as

$$\varepsilon_* = \frac{1}{J} \sum_{j=1}^J \varepsilon^{(j)} \quad (13)$$

$$\Gamma_\varepsilon = \frac{1}{J-1} \sum_{j=1}^J (\varepsilon^{(j)} - \varepsilon_*)(\varepsilon^{(j)} - \varepsilon_*)^T. \quad (14)$$

## 4. Results

In this section, we shall quantify the approximation errors in the EEG data,  
 the localization errors of the reconstructed dipoles, and subsequently, present  
 how the Bayesian uncertainty modelling can improve the localization accuracy.  
 190 In the test cases, we used single dipole sources that located in the gray matter  
 and oriented normal to the cortical surface. The EEG data was computed  
 using one of the *accurate* lead field matrices that had skull conductivity 0.0041

[23, 46, 20, 47], 0.0113, 0.0258 or 0.0330 S/m [48, 23] (denoted as  $\sigma_0 - 2\delta_{\sigma_0}$ ,  $\sigma_0 - \delta_{\sigma_0}$ ,  $\sigma_0 + \delta_{\sigma_0}$  and  $\sigma_0 + 2\delta_{\sigma_0}$ ); however, all the reconstructions with the dipole scan algorithm, using Equations (11) and (10), were performed with the same lead field matrix that had the mean skull conductivity  $\sigma_0 = 0.01855$  S/m.

#### 4.1. Approximation errors of EEG data

In order to quantify and visualize the approximation errors, i.e. the discrepancies between the EEG data computed from the accurate and standard model, we utilize the 2-norm of the normalized approximation error ( $\varepsilon_N$ ) defined as

$$\|\varepsilon_N\| = \frac{\|A(\sigma)d - A_0(\sigma_0)d\|}{\|A_0(\sigma_0)d\|}. \quad (15)$$

Figure 1 shows one saggital and axial plane of the human head, and every circle corresponds to one  $\|\varepsilon_N\|$  value computed from noiseless data by using a single dipole source. The accurate model on the top row was  $A(\sigma_0 - 2\delta_{\sigma_0})$  and  $A(\sigma_0 + 2\delta_{\sigma_0})$  in the bottom row.

#### 4.2. Localization errors of sources

Here, we show how the  $\|\varepsilon_N\|$  values result in source localization errors. Fig. 2 shows with circles the accurate locations of the sources and with arrows the locations where the source was reconstructed when the standard model (left column) and BAE (right column) were used. The colors correspond to the magnitude of the localization error. The same accurate models,  $A(\sigma_0 - 2\delta_{\sigma_0})$  and  $A(\sigma_0 + 2\delta_{\sigma_0})$ , were used to generate the data with the sources that located on the same saggital and axial planes as in Fig. 1.

Figure 3 shows how the localization errors depend on the depth (i.e. distance from scalp) of the source. The orange markers show the average localization error at a given source depth when the standard model was used and the black markers when the BAE was used in the reconstructions. The error bars illustrate the spread (standard deviation) of the localization error values.

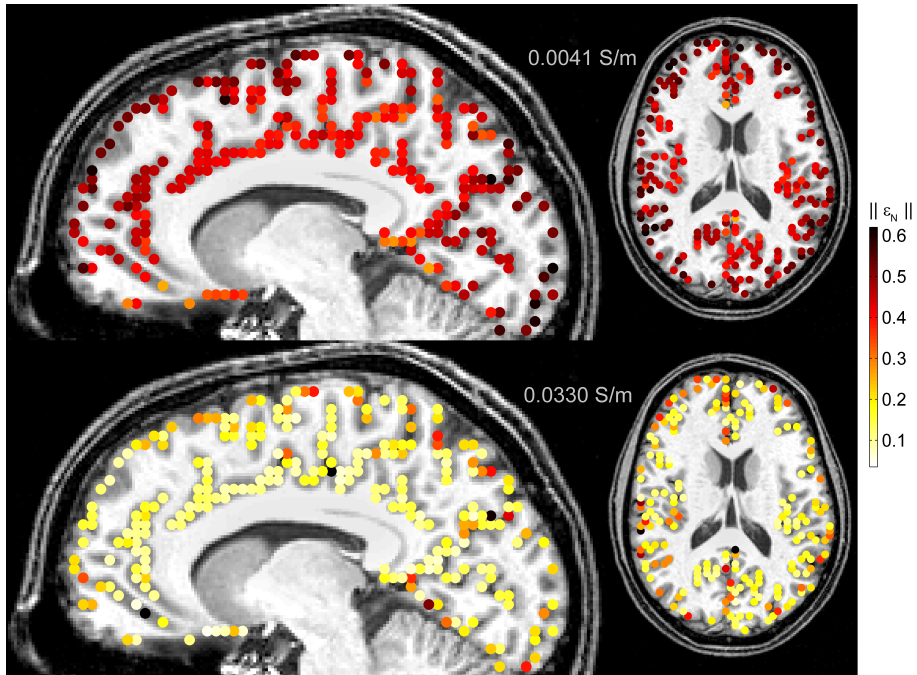


Figure 1: The 2-norm of normalized approximation error ( $\epsilon_N$ ) is shown for EEG data generated by single sources that locate in the gray matter and that are oriented normally to the cortical surface. The top row shows the  $\|\epsilon_N\|$  values when the accurate skull conductivity in the lead field model is 0.0041 S/m and the standard model has skull conductivity 0.01855 S/m. In the bottom row, the  $\|\epsilon_N\|$  values are calculated assuming that 0.033 S/m is the accurate skull conductivity.

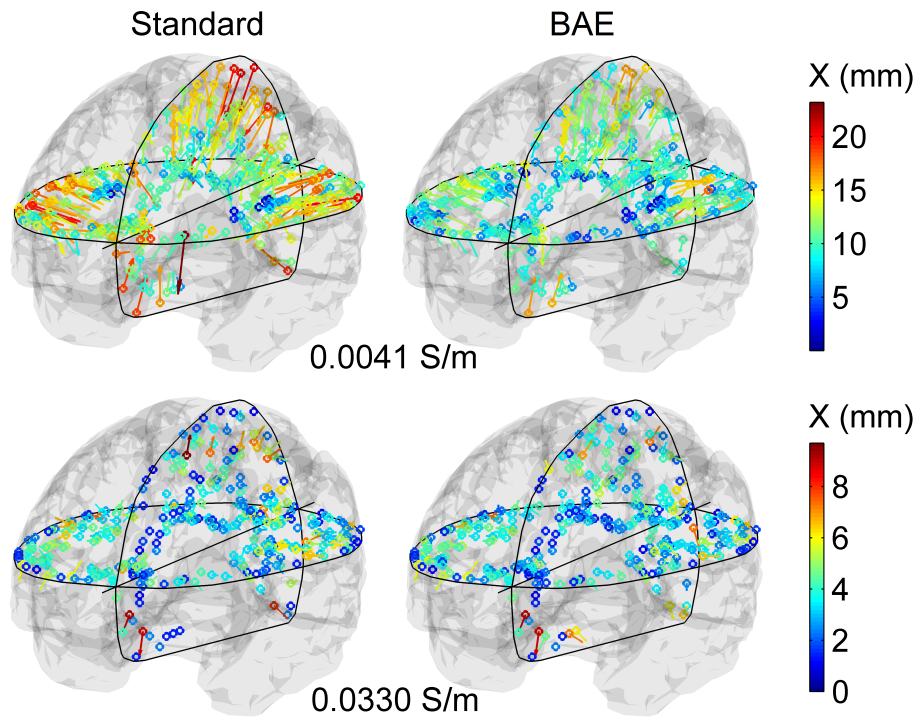


Figure 2: Top row, left: The circles show the accurate locations of the sources and the arrows show the locations of the reconstructed sources when the EEG data was generated using 0.0041 S/m skull conductivity in the lead field model and using the standard (erroneous) 0.01855 S/m skull conductivity in the reconstructions (left). Top row, right: These reconstructions were carried out using the BAE which takes statistically into account the expected variations in the unknown skull conductivity. Bottom row: The results are as above except that the EEG data was generated using 0.033 S/m skull conductivity in the lead field model.

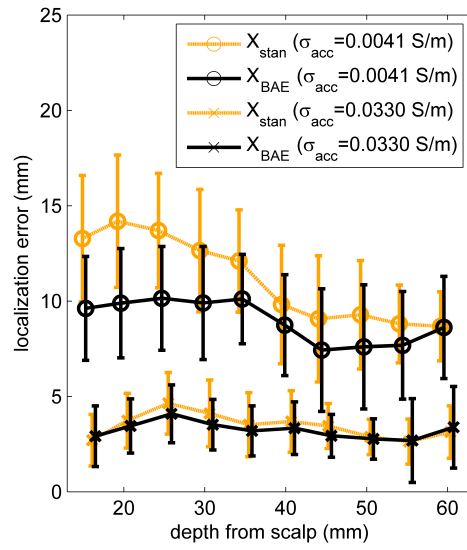


Figure 3: Localization error with respect to source depth (measured in millimeters from the scalp). The errorbars illustrate the spread (standard deviation) of the localization error values.

### 4.3. Improvement of source localization by BAE

Here, we quantify the achieved improvements in the source localization when  
220 BAE is utilized in the inverse reconstructions. The improvement is defined  
as  $\Delta = X_{\text{STAN}} - X_{\text{BAE}}$ , where  $X_{\text{STAN}}$  and  $X_{\text{BAE}}$  are the localization errors  
evaluated from solutions of the standard model (Equation (10)) and the BAE  
model (Equation (11)). In these tests, we computed the EEG forward data  
using lead field models with skull conductivities  $\sigma_0 - 2\delta\sigma_0$ ,  $\sigma_0 - \delta\sigma_0$ ,  $\sigma_0 + \delta\sigma_0$   
225 and  $\sigma_0 + 2\delta\sigma_0$  to showcase both small and large conductivity deviations from  $\sigma_0$   
that was used in all the reconstructions. Random white noise was added with  
signal-to-noise-ratios (SNR) 30 dB and 20 dB. Five different noise realizations  
for each EEG data were drawn, five reconstructions and five distance errors were  
computed, and the presented  $\Delta$  values are the corresponding averages.

230 Figure 4 presents  $\Delta$  values for the 30 dB case with varying skull conductivity  
errors.  $\Delta$  values are positive (red  $\Delta$  signs) if BAE has improved the source  
localization and negative (yellow  $\nabla$  signs) if BAE performs worse than the  
standard model. The white  $\square$  signs are used if the difference of distances is less  
than 2 mm.

235 Figure 5 shows the distributions of the  $\Delta$  values in the different skull conduc-  
tivity and SNR cases. Moreover, the average localization errors and improve-  
ments with their standard deviations are collected in Table 1. These values are  
given in millimeters between the actual and the reconstructed source for the  
accurate ( $X_{\text{ACC}}$ ), standard ( $X_{\text{STAN}}$ ) and BAE model ( $X_{\text{BAE}}$ ). The  $X_{\text{ACC}}$  are  
240 given for reference.

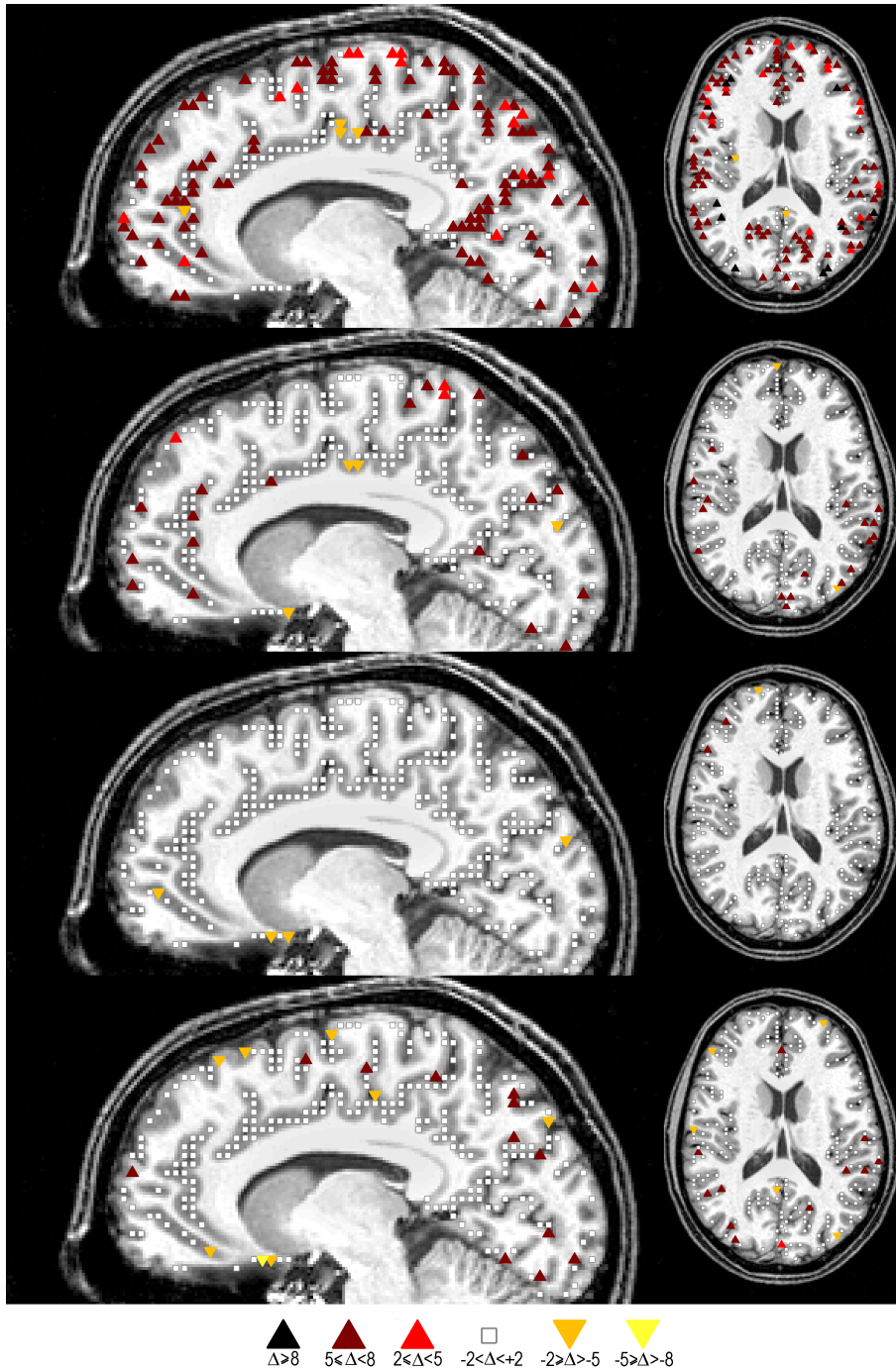


Figure 4:  $\Delta$  signs show the localization improvement (in millimeters) achieved by using BAE with respect to different skull conductivity modelling errors at SNR = 30 dB.  $\nabla$  signs are used if BAE performs worse and white  $\square$  signs if the difference of the results is less than 2 mm. In the top row, the accurate skull conductivity is 0.0041 S/m, second row 0.0113 S/m, third row 0.0258 S/m and last row 0.033 S/m whereas all the reconstructions are carried out by using the standard lead field matrix with fixed 0.01855 S/m skull conductivity.

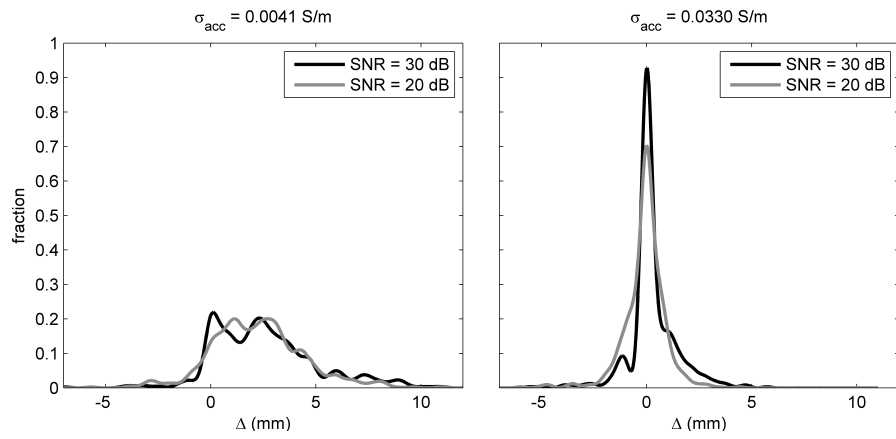


Figure 5: Left: The histograms of the improvement  $\Delta$  values in the cases when the true skull conductivity was 0.0041 S/m and SNR values 30 dB (black) and 20 dB (gray). Right: The corresponding histograms when the true skull conductivity was 0.0330 S/m.

Table 1: To evaluate the accuracy of the different solutions, we show the averages and the  $\pm 1$  standard deviations of the localization errors of the different models,  $X_{ACC}$ ,  $X_{STAN}$  and  $X_{BAE}$ , respectively, and the localization improvement  $\Delta$ .

Testing skull conductivity (S/m)	SNR (dB)	$X_{ACC}$ (mm)	$X_{STAN}$ (mm)	$X_{BAE}$ (mm)	$\Delta$ (mm)
0.0041	$\infty$	$1.7 \pm 0.5$	$12.1 \pm 3.7$	$9.4 \pm 2.9$	$2.8 \pm 3.1$
	30	$1.8 \pm 0.7$	$12.1 \pm 3.7$	$9.8 \pm 3.1$	$2.3 \pm 2.9$
	20	$2.8 \pm 1.6$	$12.2 \pm 3.9$	$10.9 \pm 3.6$	$1.3 \pm 2.5$
0.0113	$\infty$	$1.7 \pm 0.5$	$4.2 \pm 1.8$	$3.6 \pm 1.5$	$0.7 \pm 1.7$
	30	$1.8 \pm 0.7$	$4.2 \pm 1.8$	$3.7 \pm 1.6$	$0.5 \pm 1.6$
	20	$2.4 \pm 1.3$	$4.5 \pm 2.0$	$4.2 \pm 2.0$	$0.3 \pm 1.6$
0.0258	$\infty$	$1.7 \pm 0.6$	$2.6 \pm 1.1$	$2.4 \pm 1.0$	$0.2 \pm 1.0$
	30	$1.8 \pm 0.7$	$2.6 \pm 1.1$	$2.5 \pm 1.2$	$0.1 \pm 1.0$
	20	$2.2 \pm 1.1$	$3.0 \pm 1.5$	$3.0 \pm 1.6$	$0.0 \pm 1.2$
0.0330	$\infty$	$1.7 \pm 0.6$	$3.6 \pm 1.6$	$3.3 \pm 1.5$	$0.3 \pm 1.4$
	30	$1.8 \pm 0.7$	$3.6 \pm 1.6$	$3.4 \pm 1.5$	$0.2 \pm 1.4$
	20	$2.2 \pm 1.1$	$3.9 \pm 1.9$	$3.9 \pm 1.9$	$0.1 \pm 1.4$

## 5. Discussion

### 5.1. Approximation errors of EEG data

Based on Fig. 1, we can see that  $\|\varepsilon_N\|$  values are generally larger when the source is close to the skull (and the electrodes) than deep in the brain. This occurs because the electric potential, and thus also the approximation error, is inversely proportional to the distance from the source. There are few exceptions to this, i.e. cases where  $\|\varepsilon_N\|$  value is higher for a deeper source than for a superficial source, which can be either due to the curvy geometry of the GM or the discretization. As mentioned, in all the test cases the dipoles had orientations that were normal to the cortex. Now, if the local geometry is highly curvy, then two neighbouring dipoles can have very different normal orientations which lead to different EEG topographies and difference in  $\|\varepsilon_N\|$  values. Discretization, on the other hand, can have an effect on  $\|\varepsilon_N\|$  if the inverse mesh does not have enough coverage in the proximity of the forward mesh coordinates of the source. In this case, the approximation error value has a contribution from both, the conductivity difference and the discretization difference, and the BAE approach can be used to alleviate both.

With respect to the tested skull conductivity values, we see that the over-estimation of the skull conductivity ( $A(\sigma_0 - 2\delta_{\sigma_0})$  versus  $A_0(\sigma_0)$ , top row in Fig. 1) causes larger  $\|\varepsilon_N\|$  values than the under-estimation ( $A(\sigma_0 + 2\delta_{\sigma_0})$  versus  $A_0(\sigma_0)$ , bottom row in Fig. 1). This behavior is due to the fact that, in the lead field formulation, the skull conductivity is non-linearly related to the EEG data. This can be understood through an analogy to Ohm's law: If we parameterize Ohm's law with respect to conductance (or conductivity) as  $U = \frac{1}{G}I$  and deviate the conductance value by  $\delta_G$ , then  $G - \delta_G$  will always cause a larger change in  $U$  than  $G + \delta_G$  because  $U$  is proportional to the inverse of  $G$ .

### 5.2. Localization errors of sources

As can be seen from Fig. 2, the trends are that the over-estimation of skull conductivity (the top row) moves the reconstructed sources deeper in the

270 brain and under-estimation (bottom row) brings them closer to the skull. This  
 result is in agreement with literature (e.g. [51]). The over-estimation causes  
 much larger localization errors than under-estimation which is in-line with the  
 approximation errors that are also larger for the over-estimation case (see, Fig.  
 1). Therefore, it can be argued that if there is no information on the skull  
 275 conductivity and BAE cannot be used, then it is a bit safer to use a low skull  
 conductivity value rather than a high one.

When the skull conductivity is over-estimated, the sources that are close to  
 the skull present on average higher localization errors than the ones deeper in  
 the brain. This is because the deep sources cannot move further deeper in the  
 280 brain since they are already close to the bottom boundary of the source space  
 to begin with. Therefore, the deep sources exhibit smaller localization errors  
 than the shallow ones.

In the under-estimation case, the localization errors are noticeably smaller.  
 The sources that are shallow but not quite at the outer boundary have slightly  
 285 higher localization errors than the rest. Again this can be explained through  
 the geometry of the source space: the sources close to the skull have smaller  
 localization errors (than the slightly deeper ones) since they already locate close  
 to the skull (top boundary of the source space) and cannot therefore move any  
 closer.

290 This depth dependence is more evident in Fig. 3. These results are inline  
 with Fig. 1 in the sense that the localization errors are larger for the source  
 locations that also exhibit large  $\|\varepsilon_N\|$  values. BAE can improve the source  
 localization especially at points where the approximation and localization errors  
 are large for the standard model. If the localization errors are small, then  
 295 also the compensation by BAE is small and may be unnoticeable in the given  
 discretization.

### 5.3. Improvement of source localization by BAE

When the skull conductivity is over-estimated (accurate skull conductivity  
 is either  $\sigma_0 - 2\delta_{\sigma_0}$  or  $\sigma_0 - \delta_{\sigma_0}$  compared to  $\sigma_0$  in the inverse model), the localiza-

300 tion improvements are the largest. This is especially evident for SNR = 30 dB  
 and more moderate for 20 dB. The over-estimation, on average, induces higher  
 approximation errors than under-estimation (as discussed in Section 5.1). The  
 improvements gained with BAE are the highest, up to about 10 mm, for the  
 sources that locate close to the skull. This is in agreement with the locations  
 305 that exhibit the highest  $\|\varepsilon_N\|$  values.

When the skull conductivity is under-estimated (accurate skull conductivity  
 is either  $\sigma_0 + \delta_{\sigma_0}$  or  $\sigma_0 + 2\delta_{\sigma_0}$  compared to  $\sigma_0$  in the inverse model), the improve-  
 ments are smaller. On average, there are small improvements for SNR = 30 dB,  
 but for the 20 dB cases BAE gives on average similar results as the standard  
 310 model. The improvements gained with BAE are the highest for the sources  
 that locate slightly deeper in the brain (than in the over-estimation case) even  
 though the  $\|\varepsilon_N\|$  values are on average higher closer to the skull. This is be-  
 cause the under-estimation of skull conductivity shifts the sources closer to the  
 skull, and the sources that already locate close to the skull (top boundary of  
 315 the source space) cannot shift any closer.

There are some locations for which the standard model gives accurate results,  
 regardless of the erroneous skull conductivity. This occurs in such locations that  
 do not have wide support (grid points) around them. For example, when the  
 GM is highly curved there may not be additional points around the original  
 320 source location where the source could be moved.

The limit where the measurement errors start to become equal to the ap-  
 proximation errors (see, Equation (6)) occurs when the SNR drops to 20 dB.  
 This deteriorates the benefits of BAE especially in cases where the  $\|\varepsilon_N\|$  values  
 are low, and the BAE solution, Equation (10), starts to approach the solution of  
 325 the standard model, Equation (11), as the noise covariance matrix ( $\Gamma_e$ ) becomes  
 more significant.

Based on this, the consideration of the skull conductivity uncertainties by  
 utilizing BAE is the most beneficial when the SNR of the measurements is more  
 than 20 dB and it can be expected that the patient's skull conductivity may dif-  
 330 fer (significantly) from the skull conductivity that is used in the model. There-

fore, the proposed uncertainty modelling can be very useful, for example, when examining infants and young children whose skull conductivities are unknown since the value can range between several orders of magnitude [12, 52, 7]. With BAE, it is not necessary to know the exact skull conductivity, and the range of possible values can be modelled as a probability distribution. To use BAE, it is advisable to set-up this probability distribution (i.e.  $\sigma_0$  and  $\delta_{\sigma_0}$  in our case) based on age-specific literature values (e.g. [48]), then estimate the statistics of the approximation error term as described in Section 3.2, and finally add the corresponding  $\varepsilon_*$  and  $L_\varepsilon$  terms in the likelihood.

#### 5.4. *Transferability of Bayesian uncertainty modelling*

The presented BAE approach is an *a-priori* procedure in the sense that it does not require any measurement or calibration data. The BAE approach is versatile since it can be accompanied with any prior model for the sources and any (linear or non-linear) source reconstruction algorithm. Furthermore, the inclusion of BAE does not increase the complexity of the source reconstruction (as pointed out in Section 2.3) and the evaluation of the BAE statistics can be performed off-line, before any measurements are carried out.

In this paper, we chose to address the well-known problem of unknown skull conductivity. In addition to this, BAE can be used to treat other unknown (or uncertain) forward model parameters, such as the geometry of the head [36]. Moreover, the properties of the EEG electrodes are typically not modelled accurately and for instance their contact impedances are only poorly known [53, 54]. The positions of the electrodes can carry uncertainty as they are either simply assumed to be distributed according to a standard system [55] or measured by a tracking system before the EEG recording takes place. BAE is also transferable to other imaging settings, such as MEG. In MEG source analysis, a major uncertainty is the position and orientation of the head with respect to the MEG sensor coils [56, 57].

#### 5.5. *Methodological comparison to empirical Bayesian frameworks*

360 The simplicity and transferability of BAE can be highlighted when compared to empirical Bayesian frameworks [58, 59, 60, 61, 62]. In an empirical Bayesian framework, the unknown forward model parameters are also treated as stochastic variables. However, unlike in BAE, in this option these forward model parameters are estimated from the measured EEG data alongside the  
365 source activity and parameters of the prior model by maximizing the Bayesian model-evidence (or a free-energy approximation thereof) [60], or marginalized by using Bayesian model averaging [63, 64]. In other words, these are *a-posteriori* procedures since they require and depend on the EEG measurement data which is then used to estimate both the source activity and the parameters of the forward model that is exploited for the inference. This usually results in a considerably higher computational complexity compared to plain source reconstruction or BAE. In the BAE approach, the unknown forward model parameters do not need to be evaluated, it is simply enough to address their uncertainties and encapsulate them in the approximation error term. Therefore, the computational  
370 complexity of BAE is essentially the same as in the plain source reconstruction. Furthermore, as already stated, the BAE model does not depend on any measurement data, and thus is an *a-priori* procedure. In conclusion, the BAE approach can be considered as a more straightforward alternative to empirical Bayesian frameworks.

## 380 6. Conclusions and future work

We have characterized the use of Bayesian uncertainty modelling of unknown skull conductivity in EEG source imaging with respect to different skull conductivity errors and SNRs. We have shown that modelling of the skull conductivity uncertainties can reduce the source localization errors by several millimeters,  
385 and about a centimeter in the best cases. The localization accuracy improves especially when the unknown skull conductivity is over-estimated. The underestimation of the skull conductivity causes smaller localization errors, and thus the improvements are smaller as well. The highest improvements occur for the

sources that locate either close to the skull or slightly deeper in the brain, and  
390 this is in agreement with the locations that exhibit the most prominent local-  
ization errors. The benefits of BAE become uncertain when the SNR drops to  
20 dB. The proposed uncertainty modelling can be beneficial especially for in-  
fants or young children whose skull conductivities are unknown since the values  
can range between several orders of magnitude.

395 In the future studies, experimental evaluation will be carried out. In the ex-  
periments, it might be beneficial to concentrate only on a specific region of the  
brain that corresponds to a particular cognitive state or brain dysfunction. This  
anatomical restriction could further increase the localization improvements of  
BAE since the induced approximation errors will have more systematic patterns  
400 (rather than when the whole brain is considered). In the future, we will also  
study the uncertainty modelling of head geometry and skin contact in combi-  
nation with the conductivity uncertainties.

### Acknowledgement

This work was supported in parts by the Finnish Cultural Foundation (00140811),  
405 the Academy of Finland post-doctoral program (project no. 316542), IKY Fel-  
lowships of excellence for postgraduate studies in Greece - Siemens program,  
the Engineering and Physical Sciences Research Council, UK (EP/K009745/1),  
the European Union's Horizon 2020 research and innovation programme H2020  
ICT 2016-2017 under grant agreement No 732411 (as an initiative of the Photon-  
410 ics Public Private Partnership) and the Netherlands Organisation for Scientific  
Research (NWO 613.009.106/2383), EU project ChildBrain (Marie Curie Inno-  
vative Training Networks, grant agreement no. 641652) and by the Deutsche  
Forschungsgemeinschaft (DFG, project WO1425/7-1).

### References

- 415 [1] R. Brette, A. Destexhe (Eds.), Handbook of Neural Activity Measurement,  
Cambridge University Press, New York, 2012.

- [2] B. N. Cuffin, Effects of head shape on EEGs and MEGs, *IEEE Trans. Biomed. Eng.* 37 (1) (1990) 44–52. doi:10.1109/10.43614.
- [3] B. N. Cuffin, Effects of local variations in skull and scalp thickness on EEG's and MEG's, *IEEE Trans. Biomed. Eng.* 40 (1) (1993) 42–48.
- [4] G. Huiskamp, M. Vroeijsstijn, R. van Dijk, G. Wieneke, A. C. van Huf-felen, The need for correct realistic geometry in the inverse EEG problem, *IEEE Trans. Biomed. Eng.* 46 (11) (1999) 1281–1287. doi:10.1109/10.797987.
- [5] V. Montes-Restrepo, P. van Mierlo, G. Strobbe, S. Staelens, S. Vander-berghe, H. Hallez, Influence of skull modeling approaches on EEG source localization, *Brain Topogr.* 27 (2014) 95–111.
- [6] S. Vallaghé, M. Clerc, A global sensitivity analysis of three- and four-layer EEG conductivity models, *IEEE Trans. Biomed. Eng.* 56 (2009) 988–995.
- [7] H. Azizollahi, A. Aarabi, F. Wallois, Effects of uncertainty in head tissue conductivity and complexity on EEG forward modelling in neonates, *Hum. Brain Mapp.* 37 (2016) 3604–3622. doi:10.1002/hbm.23263.
- [8] M. Stenroos, A. Nummenmaa, Incorporating and compensating cere-brospinal fluid in surface-based forward models of magneto- and electroen-cephalography, *PLoS ONE* 11 (2016) e0159695.
- [9] M. Dannhauer, B. Lanfer, C. Wolters, T. Knösche, Modeling of the human skull in eeg source analysis, *Hum. Brain Mapp.* 32 (2011) 1383–1399.
- [10] K. Awada, D. Jackson, S. B. Baumann, J. Williams, D. Wilton, P. Fink, B. Prasky, Effect of conductivity uncertainties and modeling errors on EEG source localization using a 2-D model, *IEEE Trans. Biomed. Eng.* 45 (9) (1998) 1135–1145. doi:10.1109/10.709557.
- [11] S. P. van den Broek, F. Reinders, M. Donderwinkel, M. J. Peters, Volume conduction effects in EEG and MEG, *Electroenceph. Clin. Neurophysiol.* 106 (6) (1998) 522–534. doi:10.1016/S0013-4694(97)00147-8.

- 445 [12] S. Lew, D. D. Sliva, M. Choe, P. E. Grant, Y. Okada, C. H. Wolters, M. S. Hämäläinen, Effects of sutures and fontanelles on MEG and EEG source analysis in a realistic infant head model, *NeuroImage* 76 (2013) 282–293.
- [13] B. Vanrumste, G. V. Hoey, R. V. de Walle, M. D’Hav, I. Lemahieu, P. Boon, Dipole location errors in electroencephalogram source analysis due to volume conductor model errors, *Med. Biol. Eng. Comput.* 38 (5) (2000) 528–  
450 534. doi:10.1007/BF02345748.
- [14] J. Vorwerk, J.-H. Cho, S. Rampp, H. Hamer, T. R. Knösche, C. H. Wolters, A guideline for head volume conductor modeling in EEG and MEG, *NeuroImage* 100 (2014) 590–607.
- 455 [15] P. H. Laarne, M. L. Tenhunen-Eskelinen, J. K. Hyttinen, H. J. Eskola, Effect of EEG electrode density on dipole location accuracy using two realistically shaped skull resistivity models, *Brain Topogr.* 12 (2000) 249–254.
- [16] J. O. Ollikainen, M. Vauhkonen, P. A. Karjalainen, J. P. Kaipio, Effects of local skull inhomogeneities on EEG source estimation, *Med. Eng. Phys.* 21 (3) (1999) 143–154. doi:10.1016/S1350-4533(99)00038-7.  
460
- [17] P. J. Slomka, R. P. Baum, Multimodality image registration with software: state-of-the-art, *Eur. J. Nucl. Med. Mol. Imaging* 36 (1) (2009) 44–55. doi:10.1007/s00259-008-0941-8.
- [18] S. Lew, C. Wolters, A. Anwander, S. Makeig, M. R., Improved EEG source analysis using low-resolution conductivity estimation in a four-compartment finite element head model, *Human Brain Mapp.* 30 (9) (2009) 2862–2878.  
465
- [19] C. Papageorgakis, Patient specific conductivity models: characterization of the skull bones, Ph.D. thesis, Université Côte d’Azur, France (2017).
- 470 [20] M. Fuchs, M. Wagner, H. A. Wischmann, T. Köhler, A. Theissen, R. Drenckhahn, H. Buchner, Improving source reconstructions by com-

bining bioelectric and biomagnetic data, *Electroencephalogr. Clin. Neurophysiol.* 107 (2) (1998) 93–111.

- 475 [21] M. X. Huang, T. Song, D. J. H. Jr., I. Podgorny, V. Jousmaki, L. Cui, D. L. Harrington, A. M. Dale, R. R. Lee, J. Elman, E. Halgren, A novel integrated MEG and EEG analysis method for dipolar sources, *NeuroImage* 37 (3) (2007) 731–748.
- 480 [22] C. Wolters, S. Lew, R. S. MacLeod, M. Hämäläinen, Combined EEG/MEG source analysis using calibrated finite element models, *Biomedizinische Technik/Biomedical Engineering*. Rostock, Germany: Walter de Gruyter, Vol. 55 (Suppl. 1) (2010) 64–68.
- 485 [23] U. Aydin, J. Vorwerk, P. Küpper, M. Heers, H. Kugel, A. Galka, L. Hamid, J. Wellmer, C. Kellinghaus, S. Rampp, C. H. Wolters, Combining EEG and MEG for the reconstruction of epileptic activity using a calibrated realistic volume conductor model, *PLoS ONE* 9 (2014) e93154.
- 490 [24] U. Aydin, S. Rampp, A. Wollbrink, H. Kugel, J.-H. Cho, T. R. Knösche, C. Grova, J. Wellmer, C. H. Wolters, Zoomed MRI guided by combined EEG/MEG source analysis: A multimodal approach for optimizing presurgical epilepsy work-up and its application in a multi-focal epilepsy patient case study, *Brain Topogr.* 30 (2017) 417–433.
- [25] S. Goncalves, J. C. de Munck, J. P. A. Verbunt, R. M. Heethaar, F. H. L. da Silva, In vivo measurement of the brain and skull resistivities using an eit-based method and the combined analysis of sef/sep data, *IEEE Trans. Biomed. Eng.* 50 (9) (2003) 1124–1128.
- 495 [26] S. I. Goncalves, J. C. de Munck, J. P. A. Verbunt, F. Bijma, R. M. Heethaar, F. Lopes da Silva, In vivo measurement of the brain and skull resistivities using an eit-based method and realistic models for the head, *IEEE Trans. Biomed. Eng.* 50 (6) (2003) 754–767.

- [27] J. Dabek, K. Kalogianni, E. Rotgans, F. C. van der Helm, G. Kwakkel,  
500 E. E. van Wegen, A. Daffertshofer, J. C. de Munck, Determination of head  
conductivity frequency response in vivo with optimized EIT-EEG, *NeuroImage* 127 (2016) 484–495.
- [28] J. P. Kaipio, E. Somersalo, *Statistical and Computational Inverse Problems*, Applied Mathematical Series, Springer, 2004.
- [29] J. Kaipio, V. Kolehmainen, Approximate marginalization over modeling  
505 errors and uncertainties in inverse problems, in: P. Damien, N. Polson,  
D. Stephens (Eds.), *Bayesian Theory and Applications*, Oxford University  
Press, 2013.
- [30] A. Lipponen, A. Seppänen, J. P. Kaipio, Nonstationary approximation error  
510 approach to imaging of three-dimensional pipe flow: experimental evaluation,  
*Meas. Sci. Technol.* 22 (10) (2011) 104013.
- [31] A. Nissinen, L. M. Heikkinen, V. Kolehmainen, J. P. Kaipio, Compensation  
of errors due to discretization, domain truncation and unknown contact  
impedances in electrical impedance tomography, *Meas. Sci. Technol.* 20 (10)  
515 (2009) 105504.
- [32] A. Nissinen, V. Kolehmainen, J. Kaipio, Compensation of modelling errors  
due to unknown domain boundary in electrical impedance tomography,  
*IEEE Trans. Med. Imag.* 30 (2) (2011) 231–242.
- [33] S. R. Arridge, J. P. Kaipio, V. Kolehmainen, M. Schweiger, E. Somersalo,  
520 T. Tarvainen, M. Vauhkonen, Approximation errors and model reduction  
with an application in optical diffusion tomography, *Inverse Problems* 22  
(2006) 175–195. doi:10.1088/0266-5611/22/1/010.
- [34] V. Kolehmainen, M. Schweiger, I. Nissilä, T. Tarvainen, S. R. Arridge, J. P.  
Kaipio, Approximation errors and model reduction in three-dimensional  
525 diffuse optical tomography, *J. Opt. Soc. Am. A* 26 (10) (2009) 2257–2268.  
doi:10.1364/JOSAA.26.002257.

- [35] T. Tarvainen, V. Kolehmainen, A. Pulkkinen, M. Vauhkonen, M. Schweiger, S. R. Arridge, J. P. Kaipio, An approximation error approach for compensating for modelling errors between the radiative transfer equation and the diffusion approximation in diffuse optical tomography, *Inverse Problems* 26 (1) (2010) 015005. doi:10.1088/0266-5611/26/1/015005.
- 530
- [36] A. Koulouri, V. Rimpiläinen, M. Brookes, J. P. Kaipio, Compensation of domain modelling errors in the inverse source problem of the Poisson equation: Application in electroencephalographic imaging, *Appl. Num. Math.* 106 (2016) 24–36.
- 535
- [37] D. Calvetti, E. Somersalo, *Introduction to Bayesian scientific computing: Ten lectures on subjective computing*, Springer, 2007.
- [38] A. Tarantola, *Inverse problem theory and methods for model parameter estimation*, Society for Industrial and Applied Mathematics, 2007.
- [39] J. Kaipio, E. Somersalo, Statistical inverse problems: Discretization, model reduction and inverse crimes, *J. Comput. Appl. Math.* 198 (2) (2007) 493–504. doi:10.1016/j.cam.2005.09.027.
- 540
- [40] J. C. Mosher, P. S. Lewis, R. M. Leahy, Multiple dipole modeling and localization from spatio-temporal MEG data, *IEEE. Trans. Biomed. Eng.* 39 (1992) 541–557.
- 545
- [41] T. R. Knösche, *Solutions of the neuroelectromagnetic inverse problem*, Ph.D. thesis, University of Twente, The Netherlands (1997).
- [42] F. Lucka, S. Pursiainen, M. Burger, C. H. Wolters, Hierarchical Bayesian inference for the EEG inverse problem using realistic FE head models: depth localization and source separation for focal primary currents, *NeuroImage* 61 (4) (2012) 1364–1382.
- 550
- [43] C. Ramon, P. Schimpf, J. Haueisen, M. Holmes, A. Ishimaru, Role of soft bone, CSF and gray matter in EEG simulations, *Brain Topogr.* 16 (2004) 245–248.

- 555 [44] C. Ramon, P. H. Schimpf, J. Haueisen, Influence of head models on EEG simulations and inverse source localizations, *Biomed. Eng. Online* 5 (10).
- [45] S. B. Baumann, D. R. Wozny, S. K. Kelly, F. M. Meno, The electrical conductivity of human cerebrospinal fluid at body temperature, *IEEE Trans. Biomed. Eng.* 44 (1997) 220–223.
- 560 [46] S. Homma, T. Musha, Y. Nakajima, Y. Okomoto, S. Blom, R. Flink, K. E. Hagbarth, Conductivity ratios of the scalp-skull-brain head model in estimating equivalent dipole sources in human brain, *Neurosci. Res.* 22 (1) (1995) 51–55.
- [47] H. Buchner, G. Knoll, M. Fuchs, A. Rienäcker, R. Beckmann, M. Wagner,  
565 J. Silny, J. Pesch, Inverse localization of electric dipole current sources in finite element models of the human head, *Electroencephalogr. Clin. Neurophysiol.* 102 (1997) 267–278.
- [48] R. Hoekema, G. H. Wieneke, C. W. van Veelen, P. C. van Rijen, G. J. Huiskamp, J. Ansems, A. C. van Huffelen, Measurement of the conductivity  
570 of skull, temporarily removed during epilepsy surgery, *Brain Topogr.* 16 (1) (2003) 29–38.
- [49] M. Akhtari, H. C. Bryant, A. N. Mamelak, E. R. Flynn, L. Heller, J. J. Shih, M. Mandelkern, A. Matlachov, D. M. Ranken, E. D. Best, M. A. DiMauro, R. R. Lee, W. W. Sutherling, Conductivities of three-layer live  
575 human skull, *Brain Topogr.* 14 (3) (2002) 151–167.
- [50] S. Lew, C. Wolters, T. Dierkes, C. Röer, R. MacLeod, Accuracy and runtime comparison for different potential approaches and iterative solvers in finite element method based eeg source analysis, *Appl. Num. Math.* 59 (2009) 1970–1988.
- 580 [51] R. Pohlmeier, H. Buchner, G. Knoll, A. Rienäcker, R. Beckmann, J. Pesch, The influence of skull-conductivity misspecification on inverse source local-

ization in realistically shaped finite element head models, *Brain Topogr.* 9 (1997) 157–162.

- 585 [52] M. Odabae, A. Tokariev, S. Layeghy, M. Mesbah, P. B. Colditz, C. Ramon, S. Vanhatalo, Neonatal EEG at scalp is focal and implies high skull conductivity in realistic neonatal head models, *NeuroImage* 96 (2014) 73–80.
- [53] S. Pursiainen, F. Lucka, C. H. Wolters, Complete electrode model in EEG: relationship and differences to the point electrode model, *Physics in Medicine and Biology* 57 (2012) 999–1017. doi:10.1088/0031-9155/57/4/999.  
590
- [54] S. Pursiainen, B. Agsten, S. Wagner, C. H. Wolters, Advanced boundary electrode modeling for tES and parallel tES/EEG, *IEEE Trans. Neural Syst. Rehabil. Eng.* 26 (2018) 37–44.
- 595 [55] R. Oostenveld, P. Praamstra, The five percent electrode system for high-resolution EEG and ERP measurements, *Clin. Neurophysiol.* 112 (2001) 713–719.
- [56] A. Stolk, A. T. J.-M. Schoffelen, R. Oostenveld, Online and offline tools for head movement compensation in MEG, *NeuroImage* 68 (1) (2013) 39–48.
- 600 [57] S. Meyer, J. Bonaiuto, M. Lim, H. Rossiter, S. Waters, D. Bradbury, S. Bestmann, Flexible head-casts for high spatial precision MEG, *J. Neurosci. Methods* 276 (2017) 38–45.
- [58] K. Friston, L. Harrison, J. Daunizeau, S. Kiebel, C. Phillips, N. Trujillo-Barreto, R. Henson, G. Flandin, J. Mattout, Multiple sparse priors for the M/EEG inverse problem, *NeuroImage* 39 (2008) 1104–1120.  
605
- [59] R. N. Henson, J. Mattout, C. Phillips, K. J. Friston, Selecting forward models for MEG source-reconstruction using model-evidence, *NeuroImage* 46 (2009) 168–176.

- [60] S. T. Hansen, S. Hauberg, L. K. Hansen, Data-driven forward model inference for EEG brain imaging, *NeuroImage* 139 (2016) 246–258. 610
- [61] R. Henson, D. Wakeman, V. Litvak, K. Friston, A parametric empirical bayesian framework for the EEG/MEG inverse problem: Generative models for multi-subject and multi-modal integration, *Front. Hum. Neurosci.* 5 (2011) 76. doi:10.3389/fnhum.2011.00076.
- [62] G. Strobbe, P. van Mierlo, M. D. Vos, B. Mijovi, H. Hallez, S. V. Huffel, J. D. Lopez, S. Vandenberghe, Bayesian model selection of template forward models for eeg source reconstruction, *NeuroImage* 93 (2014) 11 – 22. doi: <https://doi.org/10.1016/j.neuroimage.2014.02.022>. 615
- [63] N. J. Trujillo-Barreto, E. Aubert-Vázquez, P. A. Valdés-Sosa, Bayesian model averaging in EEG/MEG imaging, *NeuroImage* 21. 620
- [64] J. D. López, W. D. Penny, J. J. Espinosa, G. R. Barnes, A general bayesian treatment for MEG source reconstruction incorporating lead field uncertainty, *NeuroImage* 60 (2012) 1194–1204.

### Appendix: Bayesian approximation error approach

In the following, we derive the likelihood terms of the Bayesian approximation error approach. 625

Let’s take the observation model as (4), and denote the total error as  $\nu = \varepsilon + e$ . Because the inverse solution is the posterior density of the Bayes’ formula  $\pi(d|v) \propto \pi(v|d)\pi(d)$ , we derive a formulation to  $\pi(v|d)$ . This is done by 630 marginalizing  $\pi(v, \nu|d)$  with respect to  $\nu$ , i.e.

$$\pi(v|d) = \int_{\nu \in \mathbb{R}^m} \pi(v, \nu|d) d\nu. \quad (16)$$

From the joint density  $\pi(v, \nu, d) = \pi(v, \nu|d)\pi(d) = \pi(v|\nu, d)\pi(\nu|d)\pi(d)$ , we obtain

$$\pi(v|d) = \int_{\nu \in \mathbb{R}^m} \pi(v|\nu, d)\pi(\nu|d)d\nu. \quad (17)$$

Now, the conditional density of  $v$  given  $d$  and  $\nu$  is obtained by using (4) as

$$\pi(v|d, \nu) = \delta(v - A_0d - \nu), \quad (18)$$

where  $\delta(\cdot)$  is the Dirac delta distribution.

635 Hence, from (18) and (17), we have that the likelihood  $\pi(v|d)$  is the convolution

$$\begin{aligned} \pi(v|d) &= \int_{\nu \in \mathbb{R}^m} \delta(v - A_0d - \nu) \pi(\nu|d) d\nu & (19) \\ &= \pi_{\nu|d}(v - A_0d|d), & (20) \end{aligned}$$

where the subscript  $\nu|d$  is used to clarify that the probability density is that of  $\nu$  given  $d$ . The measurement noise  $e \sim \mathcal{N}(e_*, \Gamma_e)$  and the approximation error term  $\varepsilon|d \sim \mathcal{N}(\varepsilon_{*|d}, \Gamma_{\varepsilon|d})$  are considered mutually uncorrelated and their distributions are approximated as Gaussian distributions. The subscript  $|d$  indicates 640 that the approximation error  $\varepsilon$  in a general case depends on  $d$ .

Thus, the approximate likelihood is a Gaussian distribution given by

$$\pi_{\nu|d}(v - A_0d|d) \propto \exp\left(-\frac{1}{2}(v - A_0d - \nu_{*|d})^T \Gamma_{\nu|d}^{-1} (v - A_0d - \nu_{*|d})\right)$$

with  $\nu_{*|d} = \varepsilon_{*|d} + e_*$  and  $\Gamma_{\nu|d} = \Gamma_{\varepsilon|d} + \Gamma_e$ .

In this paper, we use a special case of the BAE approach in which  $d$  and  $\varepsilon$  are 645 treated as mutually uncorrelated variables, i.e.  $\varepsilon \sim \mathcal{N}(\varepsilon_*, \Gamma_\varepsilon)$  (a.k.a. enhanced error model). Thus, we can write that  $\nu_* = \varepsilon_* + e_*$  and  $\Gamma_\nu = \Gamma_\varepsilon + \Gamma_e$ . We conclude to the likelihood (5). For further details on the formal derivation of the likelihood, see for example [28, 29, 33].